Original Article

Histogram analysis based on intravoxel incoherent motion diffusion-weighted imaging for determining the perineural invasion status of rectal cancer

Rong He[1#], Gesheng Song[1#], Junyi Fu[1], Weiqiang Dou[2], Aiyin Li[1^], Jingbo Chen[3]

[1]Department of Radiology, The First Affiliated Hospital of Shandong First Medical University & Shandong Provincial Qianfoshan Hospital, Jinan, China; [2]MR Research, GE Healthcare, Beijing, China; [3]Department of General Surgery, The First Affiliated Hospital of Shandong First Medical University & Shandong Provincial Qianfoshan Hospital, Jinan, China

Contributions: (I) Conception and design: R He, G Song, A Li, J Chen; (II) Administrative support: None; (III) Provision of study materials or patients: All authors; (IV) Collection and assembly of data: R He, G Song, J Fu, W Dou; (V) Data analysis and interpretation: All authors; (VI) Manuscript writing: All authors; (VII) Final approval of manuscript: All authors.

[#]These authors contributed equally to this work.

Correspondence to: Aiyin Li, MD. Department of Radiology, The First Affiliated Hospital of Shandong First Medical University & Shandong Provincial Qianfoshan Hospital, 16766 Jingshi Road, Jinan 250014, China. Email: 13953101875@139.com; Jingbo Chen, MD. Department of General Surgery, The First Affiliated Hospital of Shandong First Medical University & Shandong Provincial Qianfoshan Hospital, 16766 Jingshi Road, Jinan 250014, China. Email: qychenjingbo@163.com.

Background: Unfortunately, the morphologic magnetic resonance imaging (MRI) is unable to determine perineural invasion (PNI) status. This study applied histogram analysis of intravoxel incoherent motion diffusion-weighted imaging (IVIM-DWI) in the assessment of PNI status of rectal cancer (RC).

Methods: The retrospective analysis enrolled 175 patients with RC confirmed by postoperative pathology in The First Affiliated Hospital of Shandong First Medical University from January 2019 to December 2021. All patients underwent preoperative rectal MRI. Whole-tumor volume histogram features from IVIM-DWI were extracted using open-source software. Univariate analysis and multivariate logistic regression analysis were used to compare the differences in histogram parameters and clinical features between the PNI-positive group and PNI-negative group. Receiver operating characteristic curve analysis was used to evaluate the diagnostic performance, while the Delong test was used to compare the area under the curve of the models.

Results: The interobserver agreement of the histogram features derived from DWI, including apparent diffusion coefficient (ADC), true diffusion coefficient (D), pseudo-diffusion coefficient (D*), perfusion fraction (f), water molecular diffusion heterogeneity index (α), and distributed diffusion coefficient (DDC) were good to excellent. A total of eight histogram features including DWI_maximum, DWI_skewness, D_kurtosis, D_minimum, D_skewness, D*_energy, D*_skewness, and f_minimum were significantly different between the PNI-positive and PNI-negative groups in the univariate analysis (P<0.05); among the clinicoradiologic factors, percentage of rectal wall circumference invasion (PCI) was significantly different between the two groups (P<0.05). Multivariate analysis demonstrated that the values of D*_energy, D*_skewness, and f_minimum differed significantly between the PNI-positive patients and PNI-negative patients (P<0.05), with the independent risk factors being D*_skewness [odds ratio (OR) =1.157; 95% confidence interval (CI): 1.050–1.276; P=0.003] and PCI (OR =11.108, 95% CI: 1.767–69.838; P=0.0002). The area under the curve of the model combining the three histogram features and PCI to assess PNI status in RC

^ ORCID: 0000-0002-8342-3679.

was 0.807 (95% CI: 0.741–0.863). The results of the Delong test showed that the combined model was significantly different from each single-parameter model (P<0.05).

Conclusions: The combined model constructed on the basis of IVIM-DWI histogram features may help to assess the status of RC PNI.

Keywords: Rectal cancer (RC); perineural invasion (PNI); intravoxel incoherent motion diffusion-weighted imaging (IVIM-DWI)

Submitted Nov 13, 2023. Accepted for publication Jul 05, 2024. Published online Jul 26, 2024.
doi: 10.21037/qims-23-1614
View this article at: https://dx.doi.org/10.21037/qims-23-1614

Introduction

According to estimates from the Global Cancer Observatory 2020 (1), colorectal cancer ranks third in the world in terms of incidence and second in terms of mortality. In 2020, there were 0.7 million new cases of rectal cancer (RC) globally. The tumor- node-metastasis (TNM) classification system of the American Joint Committee on Cancer (AJCC)/Union for International Cancer Control (UICC) has been widely used in clinical risk stratification and decision-making support for RC (2,3). However, the same TNM stage may have different responses and outcomes. Therefore, accurate and individualized treatment decisions need to be supported by additional prognostic factors (4). Perineural invasion (PNI) refers to the proximity of the tumor to the nerve and encapsulation of at least 33% of the nerve circumference or penetration of tumor cells into any of the three layers of the nerve membrane (5). PNI has been proven to be significantly associated with the high recurrence rate and low survival rate in patients with RC (6-8). Previous studies have shown PNI status to be a useful indicator in guiding patients regarding the choice of preoperative and postoperative adjuvant therapy (6,9-11), and PNI-positive status may be related to the lymph node metastasis of RC (10,12). The National Comprehensive Cancer Network (NCCN) guidelines for RC list PNI as a high-risk factor for RC recurrence (2). Currently, PNI can only be confirmed by pathological examination of postoperative specimens. Therefore, an effective, noninvasive method for accurately evaluating PNI status preoperatively in patients with RC is urgently needed.

Magnetic resonance imaging (MRI) is the most commonly applied imaging modality in clinical examination for RCs. Unfortunately, morphologic MRI is unable to determine PNI status. Diffusion-weighted imaging (DWI) is a widely applied MRI technique for monitoring the diffusive movement of water molecules in living tissues and can diagnosis disease by indirectly reflecting changes in the tissue microstructure. Intravoxel incoherent motion (IVIM), via the combination of multiple small b-values and multiple high b-values, can independently reflect the true diffusion and perfusion of tissues if a biexponential model formula is applied (13). Based on the multiple b-values in IVIM-DWI, the apparent diffusion coefficient (ADC), distributed diffusion coefficient (DDC), and water molecule anisotropy (α) values can be obtained using the single-exponential model formulae and the stretched-exponential model formulae (14). IVIM-DWI has been extensively studied in the diagnosis and evaluation of rectal diseases. Examples include the diagnosis of rectal adenomas for cancer (15), the evaluation of tumor deposition (16), and the staging of lymph nodes (17). First, IVIM can provide a reference point for the identification of benign and malignant rectal lesions, tumors, and nonneoplastic lesions. Second, IVIM parameters can more sensitively reflect the histopathological features and diagnose lymph nodes status than can DWI, and some IVIM parameters showed a decreasing trend with increasing tumor stages and grades in RC (18,19). In neoadjuvant chemoradiotherapy (NCRT), the morphological changes in tumor tissues often occur later than do the microenvironmental changes, and the quantitative parameters of IVIM can reflect the microscopic characteristics in tumors more sensitively than can normal DWI (20-22). The roles that IVIM can play in other biological features of RC, such as tumor deposition, extramural vascular invasion, and neural infiltration, are the subjects of ongoing and future research.

With the extensive and in-depth research on tumor imaging, research in texture analysis is growing. Texture analysis represents a variety of mathematical methods that

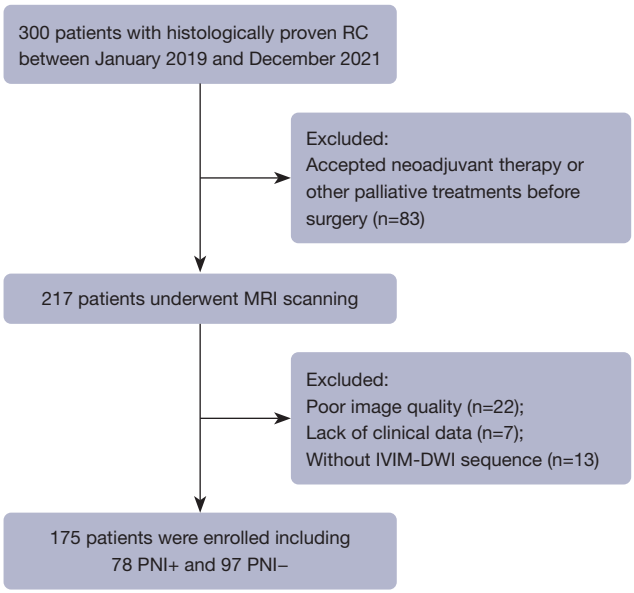

Figure 1 Flowchart of the enrolled patients. RC, rectal cancer; MRI, magnetic resonance imaging; IVIM-DWI, intravoxel incoherent motion imaging-diffusion-weighted imaging; PNI, perineural invasion.

are noninvasive that can be used to extract quantitative features from medical images to achieve objective measurements of tumor heterogeneity, thus circumventing the subjective observation errors produce by the naked eye (23-26). Quantitative features derived from grayscale intensity histograms through statistical methods are considered first-order statistics (or histogram features). These can be used to describe the distribution of signal intensity values within tumor tissue and have higher reproducibility than do higher-order texture features (24-27). In RC, histogram analysis has been applied in many research directions, including PNI status (26), nodal staging (17), distant metastasis (28), and extramural venous invasion (29). It has been reported that clinical radiomics models have the ability to predict the PNI status of RC (30,31). However, to the best of our knowledge, no studies have used IVIM-DWI-based histograms to assess PNI in RC.

Therefore, the purpose of this study was to investigate the ability of IVIM-DWI-derived primary tumor-based whole-volume histogram parameters to assess PNI status. We present this article in accordance with the STARD reporting checklist (available at https://qims.amegroups.com/article/view/10.21037/qims-23-1614/rc).

Methods

Study ethics

This study was conducted in accordance with the Declaration of Helsinki (as revised in 2013) and was approved by Medical Ethics Committee of The First Affiliated Hospital of Shandong First Medical University (Shandong Provincial Qianfoshan Hospital) (No. S537). The requirement for individual consent was waived due to the retrospective nature of the analysis.

Patients

A total of 300 patients with histologically proven RC from direct surgical resection performed between January 2019 to December 2021 were enrolled in our study. All patients underwent rectal MRI examination 1–2 weeks before surgery. The inclusion criteria were as follows: (I) adenocarcinoma confirmed by postoperative pathological biopsy, (II) standard preoperative rectal MRI examination, and (III) postoperative pathological reports including PNI status. Meanwhile, the exclusion criteria were as follows: (I) neoadjuvant therapy or other palliative treatments before surgery; (II) poor image quality, including intestinal gas or fecal artifact; (III) no IVIM-DWI; and (IV) a lack of clinical data. Finally, 175 patients were enrolled. *Figure 1* shows the flowchart of patient enrollment.

MRI acquisition

All patients underwent MRI measurements on a 3.0-T system (Discovery 750w; GE Healthcare, Chicago, IL, USA) using an eight-channel phased-array body coil in the supine position. First, fast spin-echo (FSE)-based T2-weighted imaging (T2WI) scanning was performed. Coronal FSE T2WI and oblique-axis high-resolution FSE T2WI (perpendicular to the long axis of the rectal wall where the tumor was located) were prescribed based on sagittal T2WI images. Finally, axial spin-echo echo plana image-based IVIM-DWI scanning was performed with 11 b-values applied: 0, 20, 50, 100, 150, 200, 400, 600, 800, 1,000, and 1,500 s/mm^2. The number of excitations (NEX) was 2 for b-values of 0, 20, 50, 100, 150, 200, 400, and 600 s/mm^2; 4 for b-values of 800 s/mm^2; and 6 for the b-values of 1,000 and 1,500 s/mm^2. The diffusion directions per b-value were applied in the read-out (right–left), phase (anterior–posterior), and slice (superior–inferior) directions.

Table 1 MRI parameters

Sequence	TE (ms)	TR (ms)	FOV (cm)	Thickness (mm)	Gap (mm)	Matrix	Acquisition time (s)
Sagittal T2WI	85	8,137	27	4	0.4	352×352	199
Oblique axis HR-T2WI	102	5,868	18	3	0	320×288	286
Coronal T2WI	90	7,382	32	4	0.4	480×480	231
Axial IVIM-DWI	63.7	5,000	32	5	0.5	96×128	535

Reprinted with permission from Jia *et al.* (15); https://doi.org/10.1016/j.ejrad.2022.110496. MRI, magnetic resonance imaging; TE, echo time; TR, repetition time; FOV, field of view; T2WI, T2-weighted imaging; HR, high resolution; IVIM, intravoxel incoherent motion; DWI, diffusion-weighted imaging.

The scanning sequence and parameters are listed in *Table 1*.

All patients were given a cleansing enema about 30 minutes before MRI to empty the intestinal contents and prepare the intestine; moreover, 10 mg of scopolamine was injected to reduce the motion artifacts on IVIM images via the inhibition of intestinal peristalsis. In addition, a proper amount of hypotonic contrast agent (coupling agent and water in the ratio of 1:1) was injected into the rectum through the anus before the formal scan for patients with a prepared intestine to moderately dilate the intestinal lumen and reduce the effect of gas.

MRI evaluation

Two radiologists with 15 and 8 years of experience in imaging diagnosis of rectal tumors, respectively, and who were blinded to the clinical and pathological information independently assessed the MRI findings of the tumor, including the primary site, the percentage of rectal wall circumference invasion (PCI), maximum tumor thickness, MRI-reported tumor stage (mrT), MRI-reported lymph node status (mrN), MRI-reported mesorectal fascia (mrMRF)/peritoneum status, and MRI-extramural venous invasion (mrEMVI). Any conflict of opinion was resolved via discussion. According to the distance between the primary site and the anal edge, the primary site was divided into three grades: low, medium, and high (32). TNM stage on MRI was evaluated based on the AJCC/UICC TNM staging system. The evaluation of EMVI was performed using a modified version of the 5-point scoring system devised by Jhaveri *et al.*, in which 3–4 points indicated an EMVI-positive status (33). The MRF was considered to be involved if the distance between the MRF and tumor was ≤1 mm (34).

The MRI findings of the tumor, including mrTN stage, tumor location, mrEMVI, mrMRF, and PCI, were obtained in the picture archiving and communication system (PACS). Gender, age, pathological PNI status, and preoperative laboratory parameters were recorded in the electronic medical record system. Laboratory indicators included carcinoembryonic antigen (CEA) and carbohydrate antigen 19-9 (CA19-9). The positive-PNI status was defined as the presence of tumor cells around at least one-third of the nerve circumference or in any of the three nerve layers (5).

Image postprocessing

IVIM-DWI data were imported into the Advantage Workstation 4.6 (GE HealthCare, Chicago, IL, USA), and the MADC in the Functool postprocessing toolkit (GE HealthCare, Chicago, IL, USA) was used to obtain six parameter pseudocolor maps using three model formulae. For fitting algorithms in our study, least-squares linear fitting was used in the monoexponential model, and Levenberg-Marquardt nonlinear fitting was used in the biexponential and stretched-exponential models.

(I) The monoexponential equation to acquire the ADC map is as follows: $Sb/S0 = \exp(-b \cdot ADC)$.

(II) The biexponential equation used to calculate the IVIM model and acquire the D, D*, and f maps was as follows: $Sb/S0 = (1-f)\exp(-b \cdot D) + f \exp(-b \cdot D^*)$, where D is true diffusion coefficient; D*, the pseudo-diffusion coefficient, reflects the diffusion in microcirculation; and f, the perfusion fraction, is the volume ratio of local microperfusion to the global diffusion effect in the region of interest (ROI).

(III) The stretched-exponential model was also obtained with the multi-b-value DWI to acquire the α and DDC maps as follows: $Sb/S0 = \exp[-(b \cdot DDC)\alpha]$, where α is the value 0–1 and is negatively correlated with the diffusion heterogeneity of water molecules, and DDC is the average diffusion rate.

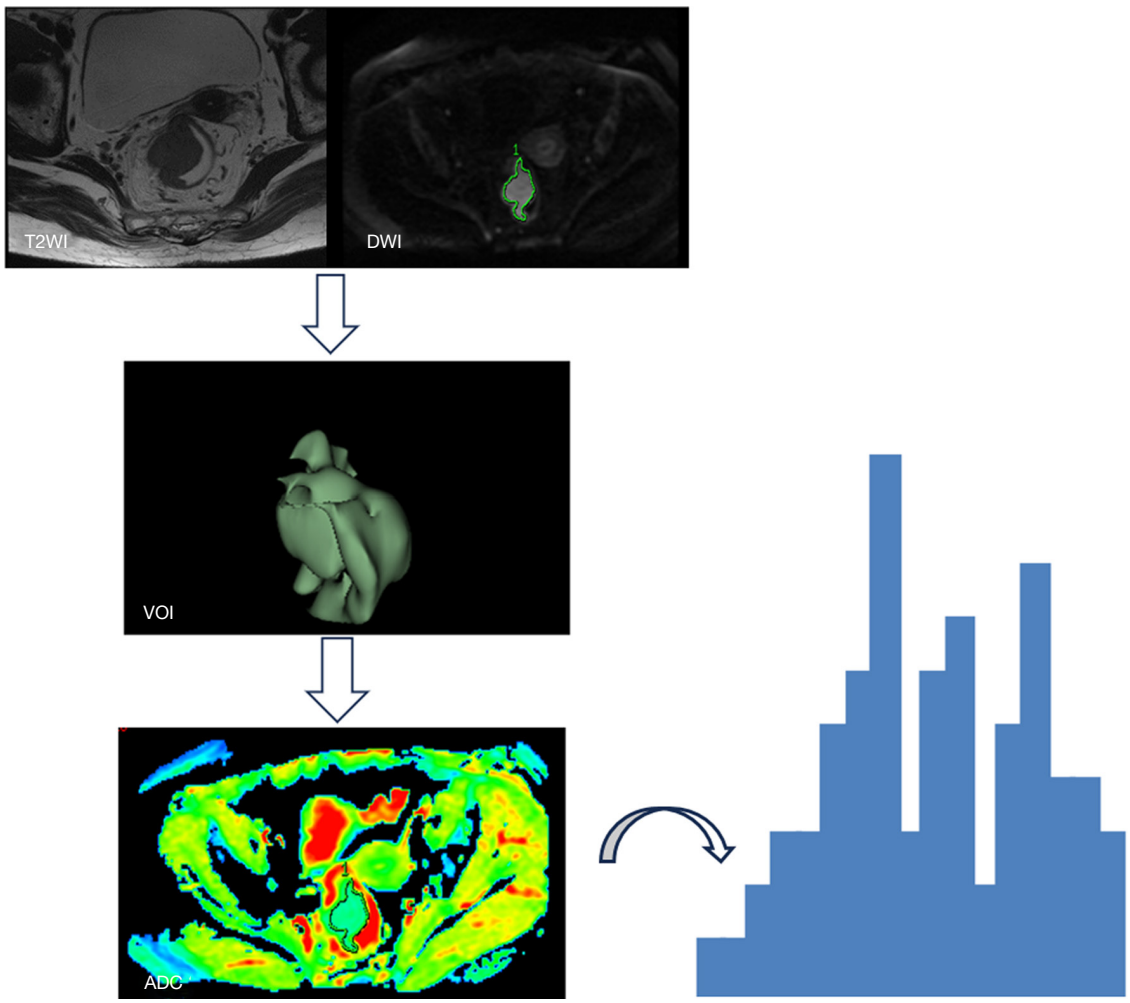

Figure 2 The process of the tumor segmentation and feature extraction. The VOIs were manually drawn along the border of the tumor on the DWI (b-value =1,000 s/mm^2) with reference to the T2WI. All VOIs were copied and pasted to functional maps. The histogram features of the whole tumor were then extracted. T2WI, T2-weighted imaging; DWI, diffusion-weighted imaging; VOIs, volumes of interest; ADC, apparent diffusion coefficient.

Tumor segmentation

The volumes of interest (VOIs) were independently measured using the open-source software, three-dimensional (3D) Slicer version 5.0.3 (www.slicer.org; in R version 30893) by two radiologists. The VOI of the tumor was manually delineated layer by layer on DWI (b-value =1,000 s/mm^2) with reference to T2WI. Subsequently, all VOIs were copied and pasted onto the parameter maps.

Histogram analysis

Software 3D Slicer was also used to extract the histogram parameters of DWI, ADC, D, D*, f, DDC, and α maps. Each diffusion parameter-specific histogram exported 18 features, including mean, minimum, maximum, 10th, median, 90th, range, interquartile range, energy, total energy, entropy, kurtosis, skewness, uniformity, variance, mean absolute deviation, robust mean absolute deviation, and root mean squared. *Figure 2* displays the process of tumor segmentation and feature extraction, and detailed definitions of the 18 first-order features are listed in *Table 2*.

Statistical analyses

All statistical analyses were performed using MedCalc

Table 2 Detailed definitions of first-order features

Feature	Explanation
Mean	The average gray-level intensity within the ROI
Minimum	Minimum = min(X)
Maximum	The maximum gray-level intensity within the ROI
10th	The 10th percentile of X
Median	The median gray-level intensity within the ROI
90th	The 90th percentile of X
Range	The range of gray values in the ROI
Interquartile range	Interquartile range = P75–P25
Energy	A measure of the magnitude of voxel values in an image
Total energy	The value of energy feature scaled by the volume of the voxel in cubic mm
Entropy	The uncertainty/randomness in the image values
Kurtosis	A measure of the "peakedness" of the distribution of values in the image ROI
Skewness	The asymmetry of the distribution of values about the mean value
Uniformity	A measure of the sum of the squares of each intensity value
Variance	The mean of the squared distances of each intensity value from the mean value
Mean absolute deviation	The mean distance of all intensity values from the mean value of the image array
Robust mean absolute deviation	The mean distance of all intensity values from the mean value calculated on the subset of image array with gray levels in between or equal to the 10th and 90th percentile
Root mean squared	The square root of the mean of all the squared intensity values

The information above has been taken from the official Pyradiomics website (https://pyradiomics.readthedocs.io/en/latest/features.html). ROI, region of interest.

(MedCalc Software, Ostend, Belgium) and SPSS 24.0 (IBM Corp., Armonk, NY, USA). Normally distributed quantitative data are presented as the mean ± standard deviation, and categorical data are expressed as the frequency (percentage). To verify interobserver agreement, intragroup correlation coefficients (ICC) for measuring histogram parameters were investigated between the two observers. Histogram characteristics and types of variables on clinical radiological characteristics were first determined, and categorical variables were analyzed using the chi-square test or Fisher exact test. The normality of the noncategorical data distribution was tested using the Kolmogorov-Smirnov test, and the independent samples *t*-test or Mann-Whitney test was used for conducting comparisons. Collinearity analysis was used to exclude parameters with severe collinearity in the univariate analysis. The association analysis of histogram features with PNI was tested using the Pearson (point-biserial correlation) test. The Z-score was used to normalize the histogram parameters before multivariable analysis. Multivariate logistic regression analysis was performed to select variables and construct models. The Hosmer-Lemeshow test was used to assess the goodness of fit of the models. Receiver operating characteristic (ROC) curve analysis was applied to evaluate diagnostic performance of each parameter and obtain the area under the ROC curve (AUC), sensitivity, specificity, and accuracy. The DeLong test was used to compare the differences in AUC between each two models. A two-sided P value <0.05 was considered statistically significant.

Results

Univariable analysis

Patient characteristics

A total of 78 patients with PNI-positive RC and 97 patients

with PNI-negative RC were included in the study. *Table 3* shows in detail the clinical and MRI characteristics of the study population based on PNI status. Age (P=0.864) and sex (P=0.289) were not statistically different, and mean age was also comparable between the two groups. However, the PNI-positive group had a higher male ratio. There was no significant difference in the distribution of preoperative embryonic CEA levels (P=0.056) and preoperative CA19-9 levels (P=0.647). Of the 78 PNI-positive patients, 53 and 40 patients were diagnosed with T3–4 and N1–2 stages on MRI images, respectively, but there were no statistical differences in T (P=0.266) or N (0.813) stages. There were also no statistical differences between the two groups in terms of EMVI (P=0.274) or MRF (P=0.572). The PCI was statistically different between the PNI-positive and PNI-negative groups (P=0.0002).

Histogram parameters

All features showed excellent or good interobserver agreement (ICC >0.8). Eight histogram features were statistically different between the PNI-positive and PNI-negative groups, including DWI_maximum (P=0.0379), DWI_skewness (P=0.0185), D_kurtosis (P=0.0416), D_minimum (P=0.0130), D_skewness (P=0.025), D*_energy (P=0.0063), D*_skewness (P=0.0081), and f_minimum (P=0.0027). Representative images are shown in *Figure 3*, while the detailed data and ROC results are listed in *Table 4*. The collinearity diagnostic output results suggested that the variance inflation factor (VIF) values of two parameters (DWI_maximum and D_minimum) were greater than 10, indicating that there was a nonnegligible collinearity problem with other parameters, and thus we excluded these two parameters. Furthermore, the remaining parameters with significant differences between the two groups were subjected to point-biserial correlation analysis. The remaining six histogram features were significantly correlated with PNI (P<0.05), and the correlation coefficients were greater than 0, indicating a positive correlation.

Multivariable analysis

Six histogram parameters (DWI_skewness, D_kurtosis, D_ skewness, D*_energy, D*_skewness, and f_minimum) and PCI were entered into the multivariate analysis which produced P values of less than 0.05 for D*_energy, D*_skewness, f_minimum, and PCI. Of these, the independent risk factors for PNI were D*_skewness [odds ratio (OR) =1.157; 95% confidence interval (CI): 1.050–1.276; P=0.003] and PCI (OR =11.108, 95% CI: 1.767–69.838; P=0.0002), and the AUC of the model established by the two indicators was relatively low, at 0.680. The ROC analyses of the statistically different single-parameter and combined-parameter models for diagnosing PNI status are detailed in *Table 5* and *Figure 4*. The multivariate binary logistic regression factors are summarized in *Table 6*. The combined model consisting of D*_energy, D*_skewness, f_minimum, and PCI achieved the best diagnostic performance, with an AUC of 0.807 (95% CI: 0.741–0.863), a sensitivity of 87.18%, a specificity of 63.92%, and an accuracy of 70.90%. In comparison, the clinical radiology (PCI) model yielded an AUC of 0.645 (95% CI: 0.569–0.715), and the histogram model (D*_energy, D*_skewness, and f_minimum)yielded an AUC of 0.776 (95% CI: 0.70–0.835). The AUC of the combined model was higher than those of each single-parameter model and histogram model. The Delong test (*Table 7*) showed that the combined model was significantly different from the single assessment model (P<0.05) but not significantly different from the histogram model. However, the combined model demonstrated improved sensitivity, sensitivity, and accuracy.

Discussion

In this study, we used histogram features extracted from DWI, ADC, D, D*, f, α and DDC maps based on IVIM-DWI and combined them with clinicoradiologic features to determine the status of PNI in RC The results showed that six histogram features and one clinicoradiologic feature were statistically different between the PNI-positive group and PNI-negative group. Further binary logistic regression analysis showed that the model combing D*_energy, D*_skewness, f_minimum, and PCI demonstrated better diagnostic performance than any single-parameter model or other combined models.

In RC, the presence and significance of PNI has been validated in numerous previous studies. PNI-positive patients have a lower disease-free survival rate at 5 years and a lower overall survival rate at 5 years than do negative patients (2). Meanwhile, other studies have concluded that PNI-positive patients with RC receiving neoadjuvant chemoradiotherapy can experience improved prognosis and survival compared with PNI-negative patients (9,35). However, the preoperative diagnosis of PNI in RC in clinic remains challenging. IVIM-DWI can simultaneously detect

Table 3 Clinical and radiological relevant data of the patients

Characteristic	Total (n=175)	PNI positive (n=78)	PNI negative (n=97)	P value
Age (years), mean ± SD	63.89±10.14	63.87±9.59	63.91±10.60	0.864
Sex, n (%)				0.289
Male	116 (66.3)	55 (70.5)	61 (62.9)	
Female	59 (33.7)	23 (29.5)	36 (37.1)	
CEA level, n (%)				0.056
<5 ng/mL	127 (72.6)	51 (65.4)	76 (78.4)	
≥5 ng/mL	48 (27.4)	27 (34.6)	21 (21.6)	
CA199 level, n (%)				0.647
<37 U/mL	159 (90.9)	70 (89.7)	89 (91.8)	
≥37 U/mL	16 (9.1)	8 (10.3)	8 (8.2)	
Tumor location, n (%)				0.884
Lower	48 (27.4)	20 (25.6)	28 (28.9)	
Middle	74 (42.3)	35 (44.9)	39 (40.2)	
Upper	53 (30.3)	23 (29.5)	30 (30.9)	
MRI T stage, n (%)				0.266
T1–2	64 (36.6)	25 (32.1)	39 (40.2)	
T3–4	111 (63.4)	53 (67.9)	58 (59.8)	
MRI N status, n (%)				0.813
N0	87 (49.7)	38 (48.7)	49 (50.5)	
N1–2	88 (50.3)	40 (51.3)	48 (49.5)	
mrEMVI, n (%)				0.274
Negative	124 (70.9)	52 (66.7)	72 (74.2)	
Positive	51 (29.1)	26 (33.3)	25 (25.8)	
mrMRF, n (%)				0.572
Negative	164 (93.7)	74 (94.9)	90 (92.8)	
Positive	11 (6.3)	4 (5.1)	7 (7.2)	
PCI, n (%)				0.0002*
<1/4	0 (0)	0 (0)	0 (0)	
1/4≤–≤1/2	105 (60.0)	36 (46.2)	69 (71.1)	
1/2<–≤3/4	63 (36.0)	39 (50.0)	24 (24.8)	
>3/4	7 (4.0)	3 (3.8)	4 (4.1)	

*, P<0.05. PNI, perineural invasion; SD, standard deviation; CEA, carcinoembryonic antigen; CA199, carbohydrate antigen 199; MRI, magnetic resonance imaging; mrEMVI, MRI-extramural venous invasion; mrMRF, MRI-reported mesorectal fascia; PCI, percentage of rectal wall circumference invaded.

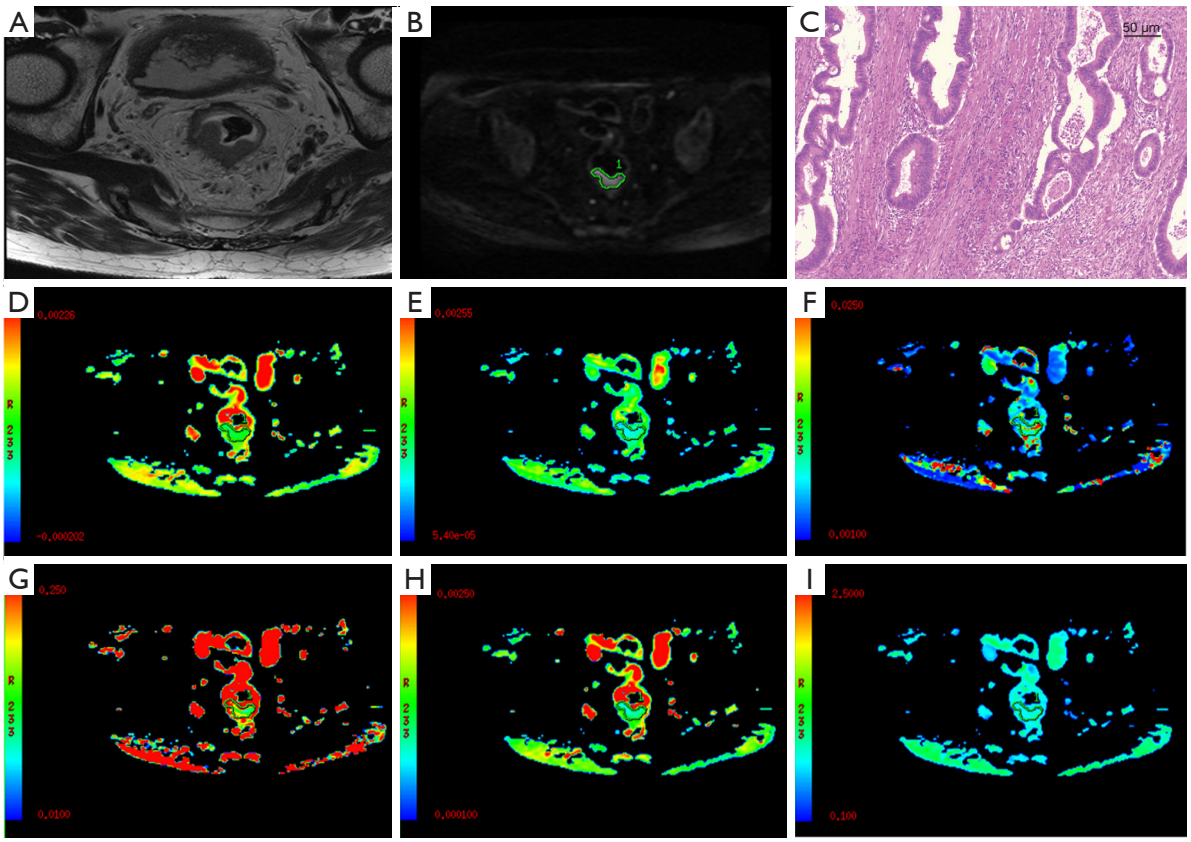

Figure 3 Representative images from a 67-year-old male patient with rectal adenoma (PNI+). VOIs are manually drawn along the border of the tumor on DWI with a b-value of 1,000 s/mm^2 and then copied to parametric maps. (A-I) Imaging of the axial T2WI, DWI, pathological map of PNI (HE image), ADC, D, D*, f, DDC, and α map, respectively. PNI, perineural invasion; VOI, volume of interest; DWI, diffusion-weighted imaging; T2WI, T2-weighted imaging; HE, hematoxylin and eosin; ADC, apparent diffusion coefficient; D, true diffusion coefficient; D*, pseudo-diffusion coefficient; f, perfusion fraction; DDC, distributed diffusion coefficient; α, water molecular diffusion heterogeneity index.

Table 4 Results of the univariate analysis and ROC analysis

Parameter	P value	AUC (95% CI)	Sensitivity (%)	Specificity (%)	Accuracy (%)
DWI_maximum	0.0379	0.589 (0.513–0.663)	58.97	57.73	56.6
DWI_skewness	0.0185	0.601 (0.524–0.674)	67.96	51.55	56.6
D_kurtosis	0.0416	0.588 (0.511–0.662)	41.03	74.23	57.7
D_minimum	0.0130	0.604 (0.528–0.677)	76.92	44.33	57.1
D_skewness	0.0250	0.596 (0.519–0.669)	83.33	38.14	55.4
D*_energy	0.0063	0.621 (0.545–0.693)	38.74	87.63	65.1
D*_skewness	0.0081	0.613 (0.537–0.686)	76.92	49.48	57.7
f_minimum	0.0027	0.624 (0.548–0.696)	75.64	45.36	60.6
PCI	0.0002	0.645 (0.569–0.715)	53.85	71.13	64.0

ROC, receiver operating characteristic curve; AUC, area under the curve; CI, confidence interval; DWI, diffusion-weighted imaging; D, true diffusion coefficient; D*, pseudo-diffusion coefficient; f, perfusion fraction; PCI, percentage of rectal wall circumference invasion.

Table 5 Diagnostic performance of individual and combined models in the diagnosis PNI of RC

Parameter	AUC (95% CI)	Sensitivity (%)	Specificity (%)	Accuracy (%)
D*_energy	0.621 (0.545–0.693)	38.74	87.63	65.1
D*_skewness	0.613 (0.537–0.686)	76.92	49.48	57.7
f_minimum	0.624 (0.548–0.696)	75.64	45.36	60.6
PCI	0.645 (0.569–0.715)	53.85	71.13	64.0
D* (energy + skewness)	0.697 (0.623–0.764)	55.13	78.35	65.7
Histogram model	0.776 (0.707–0.835)	85.90	58.76	68.6
Combined model	0.807 (0.741–0.863)	87.18	63.92	70.9

PNI, perineural invasion; RC, rectal cancer; AUC, area under the curve; CI, confidence interval; D*, pseudo-diffusion coefficient; f, perfusion fraction; PCI, percentage of rectal wall circumference invasion.

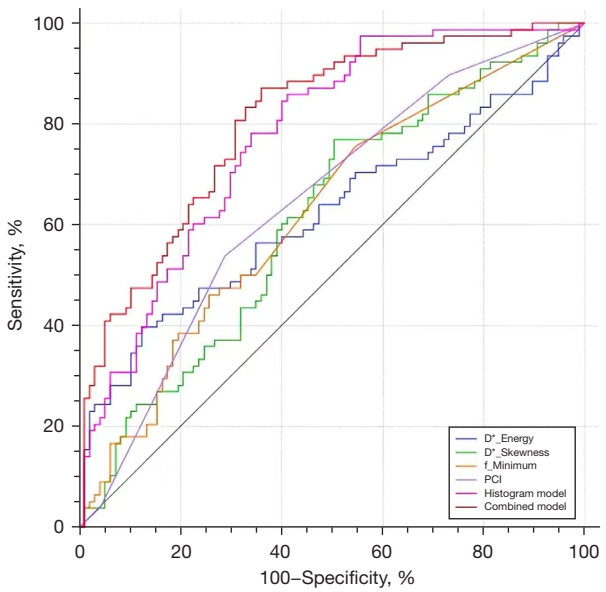

Figure 4 The receiver operating characteristics curves of models based on single and combined functional maps for diagnosing the perineural invasion status of rectal cancer. D*, pseudo-diffusion coefficient; f, perfusion fraction; PCI, percentage of rectal wall circumference invasion.

Table 6 Information of indicators included in multivariable analysis

Parameter	P	OR (95% CI)
D*_energy	<0.0001	1.000 (1.000–1.000)
D*_skewness	0.003	1.157 (1.050–1.276)
f_minimum	0.0027	1.002 (1.001–1.003)
PCI	0.0002	11.108 (1.767–69.838)

OR, odds ratio; CI, confidence interval; D*, pseudo-diffusion coefficient; f, perfusion fraction; PCI, percentage of rectal wall circumference invasion.

tissue microstructure (water molecule diffusion) and tissue microcirculation (perfusion), and IVIM has a wide range of applications in a variety of diseases including RC. However, although IVIM-DWI allows for the quantitative analysis of diffusion and perfusion, the values it acquires are averaged over all tissues within the ROI, reflecting the average characteristics in the ROI. Due to the heterogeneity of tumor tissues, the cellular distribution and tissue structure within a tumor is heterogeneous. Therefore, the trend of each characteristic value of IVIM-DWI within the ROI may also have diagnostic value. The histogram features reflect the distribution of voxel intensities within the ROI. The trends of the signals within the ROI can be discerned by analyzing each graph of IVIM-DWI through histograms. Histogram analysis and IVIM-DWI have been widely used in a variety of diseases, and their combination has frequently reported in recent studies. For example, it has been used for the identifying liver lesions (36), differentiating benign from malignant lung lesions (37), diagnosing pancreatic tumors (38), and staging lymph nodes in RC (17).

In our study, six histogram features obtained by univariable analysis were statistically different between the PNI-positive and PNI-negative groups. It indicated that the distribution of signal intensity within the VOIs from the two groups was differentiate. Further ROC evaluation revealed that the diagnostic efficiency of the individual parameters was not high. This may be due to two reasons. First, PNI is a biological phenomenon characteristic of malignant tumors. The samples in this study were all rectal adenocarcinomas that had similar biological

Table 7 The comparison of different models in the Delong test

Models	Difference between areas	Standard error	z statistic	Significance level
D* model *vs.* histogram	0.0792	0.0368	2.151	0.0315
D* model *vs.* combined	0.110	0.0387	2.853	0.0043
f_minimum *vs.* combined	0.183	0.0436	4.205	<0.0001
PCI *vs.* combined	0.162	0.0376	4.326	<0.0001
Histogram *vs.* combined	0.0312	0.0210	1.485	0.1377

D*, pseudo-diffusion coefficient; f, perfusion fraction; PCI, percentage of rectal wall circumference invasion.

and histological properties, which might have led to the diffusion and perfusion of water molecules between tumors, which, despite being heterogeneous, were not significantly different. Second, the small sample size of this study might have limited the variability. Of the clinical imaging features, only PCI was statistically different (P=0.002). The greater PCI is, the greater potential occur is for PNI. In further binary logistic regression analysis, D*_energy, D*_skewness, f_minimum, and PCI were found to be significantly different between the PNI-positive group and the PNI-negative-group, with the values of D*_energy, D*_skewness, and f_minimum being significantly higher in PNI-positive patients than in PNI-negative patients.

Energy refers to the sum of the squares of the signal intensities within the VOI. Higher D*_energy represents higher signal intensities. As a typical parameter of IVIM, D* value reflects the perfusion volume, the magnitude of which is related to the velocity of blood flow and the length of the vessel. Therefore, higher signal intensities indicate higher D* values. This suggests that the PNI-positive group had a higher level of perfusion. We speculate that this may be due to the abundant blood supply within the tumor, which increases the proliferation of tumor cells and the possibility of infiltration and metastasis, leading to an increase in the incidence of PNI. Skewness refers to the asymmetry of the gray intensity distribution of pixels in an image, and higher values of skewness indicate that the asymmetry of the normal distribution is increasing. In our study, skewness also confirmed the increased tumor heterogeneity and aggressiveness in the PNI-positive group compared to the PNI-negative group, which is in line with previous findings (26,37). Minimum represents the minimum strength in the ROI. A larger f_minimum represents greater overall perfusion intensity in the ROI and thus a richer blood supply, and this is consistent with D*_energy to a certain extent. A higher blood supply may lead to a higher probability of PNI occurrence. Regarding perfusion, an interesting recent finding is that the IVIM perfusion fraction in hepatocellular carcinomas and RCs may be affected by a prolonged T2 relaxation time, and with reduced measurements, diffusion-derived vessel density (DDVD) has the potential to be used to assess perfusion (39-41). In addition, we are also concerned that D* maps are susceptible to fitting errors. One study analyzed the accuracy and reproducibility of radiomic features computed from IVIM images using different fitting methods (42), and we will consider applying these more accurate fitting methods mentioned in our subsequent studies.

The ADC value, which reflects the free movement of water molecules in the tissue, is considered to be a potential biomarker for RC, and ADC level may reflect the invasiveness of tumors (43,44). In our study, there was no statistical difference in ADC histogram characteristics between the two groups, which may be due to the fact that the cases in this study were all malignant tumors. The total water molecular movement of the two groups was similar, and it was also affected by the number of cells, tissue microstructure, and other tissue components at the environmental level.

After multivariate logistic regression analysis, the combined model incorporating D*_energy, D*_skewness, f_minimum, and PCI had the highest AUC value (0.807). In the study of Wan *et al.* (26), their combined model (classical DWI_skewness and clinical variables) achieved an AUC value of 0.811, which is similar that in our study. However, it is worth noting that the advantages of IVIM lie in the nonenhanced diffusion and perfusion, which is more cumbersome than DWI but does provide perfusion information with diagnostic significance and is thus widely used in the preoperative diagnosis and the therapy efficacy assessment of tumors in various systems. Our study further explored the application of IVIM maps by fully

exploiting the diagnostic data of the images and by reusing the diffusion and perfusion information. Although the diagnostic energy efficiency based on IVIM in this study was not superior to that of DWI, we preliminarily proved the feasibility of the diagnosis via IVIM histograms. In the Delong test, the combined model was significantly different from each single-parameter model demonstrated higher sensitivity and accuracy as compared to the histogram model. The combined model can provide more evidence for the diagnosis of PNI and improve the diagnostic efficiency to a certain extent and does not rely solely on experience or morphological features.

Limitations

Certain limitations to this study should be addressed. First, we employed a retrospective study and included patients who had undergone direct surgical resection, whereas most patients with locally advanced disease receiving neoadjuvant therapy were excluded. Therefore, it is possible that an eligible group of participants was missed, thus introducing selection bias. Second, all patients were from the same institution. In the future, multicenter validation is necessary to extend the versatility of the histogram model. Third, the IVIM-DWI imaging we used has 11 b-values, but we could not further confirm whether it is more accurate and appropriate to use other numbers of multi-b-value IVIM, as too many b-values tend to extend the scanning time.

Conclusions

This study demonstrated that full-volume histogram parameters based on IVIM-DWI can be used to assess PNI status in RC. The combined model constructed from D*_energy, D*_skewness, f_minimum, and PCI may serve as a noninvasive tool for identifying PNI-positive status and guiding personalized patient treatment.

Acknowledgments

Funding: This work was supported by the Shandong First Medical University (Shandong Academy of Medical Sciences) Youth Science Foundation Cultivation Grant Program (grant No. 202201-080).

Footnote

Reporting Checklist: The authors have completed the STARD reporting checklist. Available at https://qims.amegroups.com/article/view/10.21037/qims-23-1614/rc

Conflicts of Interest: All authors have completed the ICMJE uniform disclosure form (available at https://qims.amegroups.com/article/view/10.21037/qims-23-1614/coif). W.D. was an employee of GE HealthCare throughout his involvement in the study. The other authors have no conflicts of interest to declare.

Ethical Statement: The authors are accountable for all aspects of the work in ensuring that questions related to the accuracy or integrity of any part of the work are appropriately investigated and resolved. This study was conducted in accordance with the Declaration of Helsinki (as revised in 2013) and was approved by Medical Ethics Committee of The First Affiliated Hospital of Shandong First Medical University (Shandong Provincial Qianfoshan Hospital) (No. S537). The requirement for individual consent was waived due to the retrospective nature of the analysis.

References

1. Sung H, Ferlay J, Siegel RL, Laversanne M, Soerjomataram I, Jemal A, Bray F. Global Cancer Statistics 2020: GLOBOCAN Estimates of Incidence and Mortality Worldwide for 36 Cancers in 185 Countries. CA Cancer J Clin 2021;71:209-49.
2. Benson AB, Venook AP, Al-Hawary MM, Azad N, Chen YJ, Ciombor KK, et al. Rectal Cancer, Version 2.2022, NCCN Clinical Practice Guidelines in Oncology. J Natl Compr Canc Netw 2022;20:1139-67.
3. Glynne-Jones R, Wyrwicz L, Tiret E, Brown G, Rödel C, Cervantes A, Arnold D; ESMO Guidelines Committee. Rectal cancer: ESMO Clinical Practice Guidelines for diagnosis, treatment and follow-up. Ann Oncol 2017;28:iv22-40.

4. Amin MB, Greene FL, Edge SB, Compton CC, Gershenwald JE, Brookland RK, Meyer L, Gress DM, Byrd DR, Winchester DP. The Eighth Edition AJCC Cancer Staging Manual: Continuing to build a bridge from a population-based to a more "personalized" approach to cancer staging. CA Cancer J Clin 2017;67:93-9.
5. Liebig C, Ayala G, Wilks JA, Berger DH, Albo D. Perineural invasion in cancer: a review of the literature. Cancer 2009;115:3379-91.
6. Stojkovic Lalosevic M, Milovanovic T, Micev M, Stojkovic M, Dragasevic S, Stulic M, Rankovic I, Dugalic V, Krivokapic Z, Pavlovic Markovic A. Perineural invasion as a prognostic factor in patients with stage I-III rectal cancer - 5-year follow up. World J Gastrointest Oncol 2020;12:592-600.
7. Kim S, Huh JW, Lee WY, Yun SH, Kim HC, Cho YB, Park YA, Shin JK. Correction to: Lymphovascular invasion, perineural invasion, and tumor budding are prognostic factors for stage I colon cancer recurrence. Int J Colorectal Dis 2020;35:1171.
8. Nikberg M, Chabok A, Letocha H, Kindler C, Glimelius B, Smedh K. Lymphovascular and perineural invasion in stage II rectal cancer: a report from the Swedish colorectal cancer registry. Acta Oncol 2016;55:1418-1424.
9. Sung SY, Kim SH, Jang HS, Song JH, Jeong S, Jung JH, Lee JH. Pathologic Implications of Radial Resection Margin and Perineural Invasion to Adjuvant Chemotherapy after Preoperative Chemoradiotherapy and Surgery for Rectal Cancer: A Multi-Institutional and Case-Matched Control Study. Cancers (Basel) 2022;14:4112.
10. Song JH, Yu M, Kang KM, Lee JH, Kim SH, Nam TK, Jeong JU, Jang HS, Lee JW, Jung JH. Significance of perineural and lymphovascular invasion in locally advanced rectal cancer treated by preoperative chemoradiotherapy and radical surgery: Can perineural invasion be an indication of adjuvant chemotherapy? Radiother Oncol 2019;133:125-31.
11. Kim CH, Yeom SS, Lee SY, Kim HR, Kim YJ, Lee KH, Lee JH. Prognostic Impact of Perineural Invasion in Rectal Cancer After Neoadjuvant Chemoradiotherapy. World J Surg 2019;43:260-72.
12. Xu Y, Chen Y, Long C, Zhong H, Liang F, Huang LX, Wei C, Lu S, Tang W. Preoperative Predictors of Lymph Node Metastasis in Colon Cancer. Front Oncol 2021;11:667477.
13. Le Bihan D, Breton E, Lallemand D, Grenier P, Cabanis E, Laval-Jeantet M. MR imaging of intravoxel incoherent motions: application to diffusion and perfusion in neurologic disorders. Radiology 1986;161:401-7.
14. Iima M. Perfusion-driven Intravoxel Incoherent Motion (IVIM) MRI in Oncology: Applications, Challenges, and Future Trends. Magn Reson Med Sci 2021;20:125-38.
15. Jia Y, Song G, Wu R, Hong Y, Dou W, Li A. Intravoxel incoherent motion DWI with different mathematical models in predicting rectal adenoma with and without canceration. Eur J Radiol 2022;155:110496.
16. Hong Y, Song G, Jia Y, Wu R, He R, Li A. Predicting tumor deposits in patients with rectal cancer: Using the models of multiple mathematical parameters derived from diffusion-weighted imaging. Eur J Radiol 2022;157:110573.
17. Zhao L, Liang M, Yang Y, Zhao X, Zhang H. Histogram models based on intravoxel incoherent motion diffusion-weighted imaging to predict nodal staging of rectal cancer. Eur J Radiol 2021;142:109869.
18. Surov A, Meyer HJ, Höhn AK, Behrmann C, Wienke A, Spielmann RP, Garnov N. Correlations between intravoxel incoherent motion (IVIM) parameters and histological findings in rectal cancer: preliminary results. Oncotarget 2017;8:21974-21983.
19. Sun H, Xu Y, Song A, Shi K, Wang W. Intravoxel Incoherent Motion MRI of Rectal Cancer: Correlation of Diffusion and Perfusion Characteristics With Prognostic Tumor Markers. AJR Am J Roentgenol 2018;210:W139-47.
20. Lu W, Jing H, Ju-Mei Z, Shao-Lin N, Fang C, Xiao-Ping Y, Qiang L, Biao Z, Su-Yu Z, Ying H. Intravoxel incoherent motion diffusion-weighted imaging for discriminating the pathological response to neoadjuvant chemoradiotherapy in locally advanced rectal cancer. Sci Rep 2017;7:8496.
21. Xu Q, Xu Y, Sun H, Chan Q, Shi K, Song A, Wang W. Quantitative intravoxel incoherent motion parameters derived from whole-tumor volume for assessing pathological complete response to neoadjuvant chemotherapy in locally advanced rectal cancer. J Magn Reson Imaging 2018;48:248-58.
22. Dolciami M, Capuani S, Celli V, Maiuro A, Pernazza A, Palaia I, Di Donato V, Santangelo G, Rizzo SMR, Ricci P, Della Rocca C, Catalano C, Manganaro L. Intravoxel Incoherent Motion (IVIM) MR Quantification in Locally Advanced Cervical Cancer (LACC): Preliminary Study on Assessment of Tumor Aggressiveness and Response to Neoadjuvant Chemotherapy. J Pers Med 2022;12:638.
23. Gatenby RA, Grove O, Gillies RJ. Quantitative imaging in cancer evolution and ecology. Radiology 2013;269:8-15.

24. Castellano G, Bonilha L, Li LM, Cendes F. Texture analysis of medical images. Clin Radiol 2004;59:1061-9.
25. Davnall F, Yip CS, Ljungqvist G, Selmi M, Ng F, Sanghera B, Ganeshan B, Miles KA, Cook GJ, Goh V. Assessment of tumor heterogeneity: an emerging imaging tool for clinical practice? Insights Imaging 2012;3:573-89.
26. Wan L, Peng W, Zou S, Shi Q, Wu P, Zhao Q, Ye F, Zhao X, Zhang H. Predicting perineural invasion using histogram analysis of zoomed EPI diffusion-weighted imaging in rectal cancer. Abdom Radiol (NY) 2022;47:3353-63.
27. Gourtsoyianni S, Doumou G, Prezzi D, Taylor B, Stirling JJ, Taylor NJ, Siddique M, Cook GJR, Glynne-Jones R, Goh V. Primary Rectal Cancer: Repeatability of Global and Local-Regional MR Imaging Texture Features. Radiology 2017;284:552-61.
28. Boca Petresc B, Caraiani C, Popa L, Lebovici A, Feier DS, Bodale C, Buruian MM. The Utility of ADC First-Order Histogram Features for the Prediction of Metachronous Metastases in Rectal Cancer: A Preliminary Study. Biology (Basel) 2022;11:452.
29. Chen W, Liu G, Chen J, Wei Q, Ye Y, Du X, Feng J, Yan Z, Deng K, Liu X. Whole-tumor amide proton transfer-weighted imaging histogram analysis to predict pathological extramural venous invasion in rectal adenocarcinoma: a preliminary study. Eur Radiol 2023;33:5159-71.
30. Zhang K, Ren Y, Xu S, Lu W, Xie S, Qu J, Wang X, Shen B, Pang P, Cai X, Sun J. A clinical-radiomics model incorporating T2-weighted and diffusion-weighted magnetic resonance images predicts the existence of lymphovascular invasion / perineural invasion in patients with colorectal cancer. Med Phys 2021;48:4872-82.
31. Guo Y, Wang Q, Guo Y, Zhang Y, Fu Y, Zhang H. Preoperative prediction of perineural invasion with multi-modality radiomics in rectal cancer. Sci Rep 2021;11:9429.
32. Nicholls RJ, Zinicola R, Haboubi N. Extramural spread of rectal cancer and the AJCC Cancer Staging Manual 8th edition, 2017. Ann Oncol 2019;30:1394-5.
33. Jhaveri KS, Hosseini-Nik H, Thipphavong S, Assarzadegan N, Menezes RJ, Kennedy ED, Kirsch R. MRI Detection of Extramural Venous Invasion in Rectal Cancer: Correlation With Histopathology Using Elastin Stain. AJR Am J Roentgenol 2016;206:747-55.
34. Beets-Tan RGH, Lambregts DMJ, Maas M, Bipat S, Barbaro B, Curvo-Semedo L, Fenlon HM, Gollub MJ, Gourtsoyianni S, Halligan S, Hoeffel C, Kim SH, Laghi A, Maier A, Rafaelsen SR, Stoker J, Taylor SA, Torkzad MR, Blomqvist L. Magnetic resonance imaging for clinical management of rectal cancer: Updated recommendations from the 2016 European Society of Gastrointestinal and Abdominal Radiology (ESGAR) consensus meeting. Eur Radiol 2018;28:1465-75.
35. Kim YI, Kim CW, Kim JH, Kim J, Ro JS, Lee JL, Yoon YS, Park IJ, Lim SB, Yu CS, Kim JC. Clinical Implication of Perineural and Lymphovascular Invasion in Rectal Cancer Patients Who Underwent Surgery After Preoperative Chemoradiotherapy. Dis Colon Rectum 2022;65:1325-34.
36. Ai Z, Han Q, Huang Z, Wu J, Xiang Z. The value of multiparametric histogram features based on intravoxel incoherent motion diffusion-weighted imaging (IVIM-DWI) for the differential diagnosis of liver lesions. Ann Transl Med 2020;8:1128.
37. Li J, Wu B, Huang Z, Zhao Y, Zhao S, Guo S, Xu S, Wang X, Tian T, Wang Z, Zhou J. Whole-lesion histogram analysis of multiple diffusion metrics for differentiating lung cancer from inflammatory lesions. Front Oncol 2022;12:1082454.
38. Li J, Liang L, Yu H, Shen Y, Hu Y, Hu D, Tang H, Li Z. Whole-tumor histogram analysis of non-Gaussian distribution DWI parameters to differentiation of pancreatic neuroendocrine tumors from pancreatic ductal adenocarcinomas. Magn Reson Imaging 2019;55:52-9.
39. Lu BL, Yao DQ, Wáng YXJ, Zhang ZW, Wen ZQ, Xiao BH, Yu SP. Higher perfusion of rectum carcinoma relative to tumor-free rectal wall: quantification by a new imaging biomarker diffusion-derived vessel density (DDVD). Quant Imaging Med Surg 2024;14:3264-74.
40. Li XM, Yao DQ, Quan XY, Li M, Chen W, Wáng YXJ. Perfusion of hepatocellular carcinomas measured by diffusion-derived vessel density biomarker: Higher hepatocellular carcinoma perfusion than earlier intravoxel incoherent motion reports. NMR Biomed 2024;37:e5125.
41. Ma FZ, Wáng YXJ. T2 relaxation time elongation of hepatocellular carcinoma relative to native liver tissue leads to an underestimation of perfusion fraction measured by standard intravoxel incoherent motion magnetic resonance imaging. Quant Imaging Med Surg 2024;14:1316-22.
42. Scalco E, Rizzo G, Mastropietro A. The quantification of IntraVoxel incoherent motion - MRI maps cannot preserve texture information: An evaluation based on simulated and in-vivo images. Comput Biol Med 2023;154:106495.
43. Sun Y, Tong T, Cai S, Bi R, Xin C, Gu Y. Apparent

Diffusion Coefficient (ADC) value: a potential imaging biomarker that reflects the biological features of rectal cancer. PLoS One 2014;9:e109371.
44. Curvo-Semedo L, Lambregts DM, Maas M, Beets GL, Caseiro-Alves F, Beets-Tan RG. Diffusion-weighted MRI in rectal cancer: apparent diffusion coefficient as a potential noninvasive marker of tumor aggressiveness. J Magn Reson Imaging 2012;35:1365-71.

Cite this article as: He R, Song G, Fu J, Dou W, Li A, Chen J. Histogram analysis based on intravoxel incoherent motion diffusion-weighted imaging for determining the perineural invasion status of rectal cancer. Quant Imaging Med Surg 2024;14(8):5358-5372. doi: 10.21037/qims-23-1614

